Journal of Materials Chemistry B

ROYAL SOCIETY OF CHEMISTRY

PAPER

View Article Online
View Journal | View Issue

Cite this: *J. Mater. Chem. B*, 2024, **12**, 12050

Collagen nanobubbles as efficient carriers for targeted controlled release of ibrutinib†

Sena Pişkin,‡[a] Handan Sevim Akan,[b] Canan Armutcu[a] and Lokman Uzun *[a]

Received 23rd July 2024,
Accepted 7th October 2024

DOI: 10.1039/d4tb01608d

rsc.li/materials-b

Nanobubbles are designed to increase structural stability and enhance the distribution of the transported drug to the targeted site. They can efficiently penetrate the desired area from the bloodstream due to the small size of nanobubbles. In general, the structure of the bubbles contains a gas inside, surrounded by an outer polymeric shell. In this study, perfluoropentane was utilized as a gaseous core whereas collagen was used to form shells because of its biodegradability and excellent biocompatibility. The release studies of collagen nanobubbles prepared at several drug doses were carried out in a Franz cell using a dialysis membrane at different pH (5.5–7.4) and temperature (4.0–40.0 °C) ranges. In the release experiments with collagen nanobubbles, it was observed that approximately 70% of the drug was released within 6 days at pH 7.4 whereas the same releasing rate was achieved within only 24 h after exploding by ultrasound treatment. At the same time, a cytotoxicity study was carried out to demonstrate the effectiveness of the synthesized nanobubbles. With increasing drug loading concentration and ultrasound treatment, the cytotoxic activities of nanobubbles became similar to those of the free drug (ibrutinib). Furthermore, cell culture studies were performed to assess *in vitro* drug-releasing efficiencies of nanobubbles by using the HeLa cell line as a model of soft cancer tissue. In conclusion, these nanobubbles could be classified as an efficient alternative to carrying active agents for treating soft tissue tumors.

1. Introduction

Drug delivery systems aim to transport the active substance throughout the body to achieve the intended therapeutic effect. Moreover, targeted/controlled drug release is a technique that allows a drug to be released to the desired area in the body for a desired time and dose.[1,2] Herein, the drug must be physically or chemically attached to the material called the scaffold.[3] Release of the drug can sometimes occur either through adjustable degradation of the scaffold or sometimes by diffusion. Therefore, it is possible to regulate the amount of the drug released by many parameters such as the chemical and physical properties of the scaffold, the distribution method, and the application methods of the drug.[4]

Because cancer is one of the diseases with the highest mortality rate in the world, many treatment methods have been proposed including surgery, radiotherapy, chemotherapy, immunotherapy, and a combination of these.[5] Chemotherapy is used in the first stage of treatment although it has disadvantages such as not being able to fully target the desired area and not achieving the acceptable therapeutic effect. On the other hand, insufficient solubility of chemotherapeutic drugs used in treatment also causes limited biodistribution, decreased bioavailability, and poor pharmacokinetic properties.[6]

Ibrutinib (IBR) is a potent orally administered therapeutic that acts *via* irreversible inhibition of Bruton's tyrosine kinase (BTK).[7] Due to its inhibition efficiency, IBR has gained importance in the last decade for the treatment of mantle cell lymphoma (MCL) and chronic lymphocytic leukemia (CLL).[8] Unfortunately, it has both very low solubility in water and bioavailability at only 3%.[9] Considering this situation, higher doses of IBR are required to achieve the desired therapeutic effect. However, high-dose drugs cause increased toxicity and side effects. As is well known, chemotherapeutics administered in higher doses not only kill cancer cells but also damage healthy tissues.[10] In this respect, researchers focused their attention on medical applications to treat cancer safely and more effectively, and nanotechnology has provided an opportunity to design delivery systems containing the drug to be used.[11]

Nanobubbles, gas-containing spherical materials surrounded by an outer shell, are considered an alternative nanocarrier for drug release studies with a size range of less than 1 μM in

[a] *Hacettepe University, Faculty of Science, Department of Chemistry, Biochemistry Division, 06800-Beytepe, Ankara, Turkey. E-mail: lokman@hacettepe.edu.tr; Tel: +90312 297 7337*

[b] *Hacettepe University, Faculty of Science, Department of Biology, Ankara, Turkey*

† Electronic supplementary information (ESI) available. See DOI: https://doi.org/10.1039/d4tb01608d

‡ This study is part of her master of science study.

aqueous solution.[12,13] Nanobubbles have attracted great attention due to their promising features such as structural stability, small size, high surface-to-volume ratio, long life, and acoustic properties.[12,14] In relation to biomedical applications, nanobubbles exhibit sensitivity and responsibility to environmental/external stimuli including ultrasound waves, light, and changes in pH.[15,16] Accordingly, nanobubbles enable a variety of biomedical applications such as ultrasound imaging, drug delivery, and therapy in biomedical applications.[10,11,17] On the other hand, polymers (both synthetic and natural), lipids, and proteins have been utilized to provide targeted delivery to the site of interest, both using novel therapeutic anti-cancer agents and adjustable and controlled release of these therapeutics.[18] It has also been shown in many studies that these materials increase the effectiveness of cancer treatment and significantly reduce side effects.

Collagen, one of the most preferred biopolymers, is a protein found abundantly in the human body, especially in skin and bone tissue. There are several important reasons for the effectiveness of collagen in drug delivery systems in cancer.[19–21] Firstly, the fact that cancer cells contain more integrin receptors makes the use of collagen advantageous[22] because integrins promote the development of integrin-antagonist molecules that impair tumor growth of both tumor cells and tumor-associated cells, particularly endothelial cells.[23,24] Secondly, collagen contains the arginine–glycine–aspartic acid (RGD) repeating tripeptide recognition site.[25] RGD sequences are recognized by integrins, and this specific recognition takes collagen one step further in drug delivery systems, particularly in cancer treatments. Using this feature, collagen plays a major and efficient role in passively targeting tumor tissue without any need to immobilize functional groups or affinity ligands such as small molecules, receptors, enzymes, or antibodies.

In this study, we focused our attention on developing a targeted controlled drug-carrying system using nanobubbles for the therapeutic efficiency of IBR. To this aim, collagen nanobubbles were synthesized by the two-surfactant emulsion formation method using lecithin and palmitic acid with perfluoropentane as a gaseous core. Synthesized collagen nanobubbles were characterized by using scanning electron microscopy (SEM), Fourier transform infrared (ATR-FTIR), zeta size, and potential measurements. Controlled drug-release studies were performed through two different approaches including with/without ultrasound treatment in order to show the effects of exploding those nanobubbles on drug-releasing kinetics. Moreover, the cytotoxicity of nanobubbles was assessed by performing cell-culture studies with an L929 cell line as healthy cells and a HeLa cell line as a model of soft cancer tissue *via* MTT assay.

2. Materials and methods

2.1. Chemicals

To form the outer shell of the nanobubbles, collagen was used after being obtained from Collagen Solutions Ltd (Glasgow, Scotland). Perfluoropentane (gas to fill the nanobubbles), lecithin, palmitic acid, sodium dihydrogen phosphate, sodium phosphate, sodium hydroxide, and hydrochloric acid were obtained from Sigma-Aldrich (Maryland, USA). Ethanol was supplied from Isolab (Eschau, Germany), and Pluronic-F68 was used as a stabilizing agent and obtained from Thermo Fisher (Waltham, USA). Ibrutinib was provided by TOBIO Pharmaceuticals (Istanbul, Turkiye). Biotech dialysis membrane (12–14 kDa) was used for release studies. All other chemicals were of analytical standard and used as received. Deionized water used in all steps has a conductivity of 18 MΩ.

2.2. Preparation of collagen nanobubbles

Collagen nanobubbles were synthesized *via* the two-surfactant emulsion formation method. Briefly, lecithin, one of the surfactants to produce the emulsion was dissolved in absolute ethanol to obtain a concentration of 3% (w/v). After that, palmitic acid, the second surfactant was added to the lecithin solution at a final concentration of 0.3% (w/v) and dissolved at room temperature whereas the final ethanol content was 4.7% (w/v) in the final solution. While stirring at 250 rpm at room temperature, ibrutinib (in four different amounts in the range of 1.0–4.0 mg) was added to the previous solution and completely dissolved. Furthermore, the absorbance value of the resulting solution was measured with a spectrophotometer (at a wavelength of 260 nm) to calculate the recovery. Perfluoropentane (2.196 mL) was then added to this solution and deionized water (12.47 mL) was added until a milky emulsion was formed. This mixture was placed in an ice bath and homogenized using an ultrasonicator at 12 000 rpm for 3 min (Fig. 1). During this step, the solution was removed from the ice bath, and subsequent stirring continued with a mechanical mixer at 90 rpm at room temperature for 5 min. In order to wrap the micelles, collagen solution (2%, w/v in deionized water) was added dropwise meanwhile applying continuously stirring the solution for a while. An aqueous solution of 0.01% Fluronic-F68 was then added as a stabilizing agent. The resulting bubbles were washed three times with deionized water while centrifuging them at 10 000 rpm at 10 °C for 15 min. Herein, the supernatant was removed from the nanobubbles which precipitated at the bottom. In order to calculate the drug loading efficiency/capacity performances, washing-out solutions were collected after centrifugation to quantify the IBR *via* spectrophotometric measurements. The resulting nanobubbles were filtered with 0.45 μm, and 0.22 μm CA (cellulose acetate) membrane filters, respectively, and stored at +4.0 °C.

2.3. Structural analyses

Morphological structure analyses of nanobubbles were performed by scanning electron microscopy (TESCAN GAIA 3, Brn-Kohoutovice, Czech Republic). Approximately, 10 μL of nanobubble samples were dropped on double-sided carbon tape, dried in open air, and then analyzed after coating with a thin gold layer. The attenuated total reflection-Fourier transform infrared (ATR-FTIR) spectrophotometer (Scattered Reflection, Thermo model-Nicolet-IS 10 FTIR) was used to characterize the

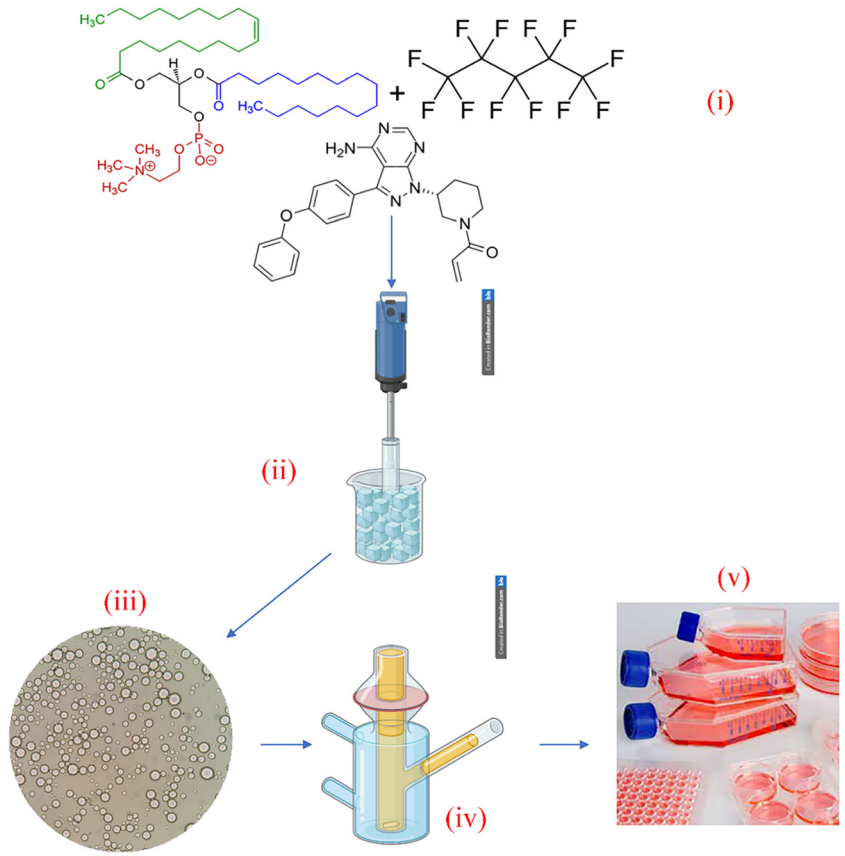

Fig. 1 A schematic representation of the flow chart for experimental steps. (i) Preparation of the solutions; (ii) homogenization in an ice-bath; (iii) checking the nanobubble formation and subsequent filtration; (iv) drug release analysis *via* a Franz cell; and (v) cell culture for cytotoxicity analysis.

functional groups of the nanobubbles. Herein, the nanobubbles were dropped on a glass surface and dried prior to measurement. Particle size and zeta-surface charge were measured to assess the effects of the drug loading on the surface charge and size of the synthesized nanobubbles (Malvern Zetasizer Nano-ZS ZEN 3600).

2.4. Drug loading capacity/efficiency

In order to calculate the rate of drug loading into the nanobubbles, the spectrometric measurements (Shimadzu UV-mini 1240 UV-Vis spectrophotometer) were performed at 260 nm. Before performing the measurements on starting and washing-out solutions, a series of standard IBR solutions were prepared to obtain a calibration curve while drawing a curve of concentration *vs.* absorbance. By using the equation for the calibration curve, the amounts of drug molecules in these solutions were calculated whereas drug-loading efficiency was measured by using suitable mass-balances.

2.5. Drug release studies

In order to determine the drug release profiles of ibrutinib-loaded nanobubbles before and after the ultrasonic treatment, release studies were performed while evaluating the effects of the parameters concerning pH (5.5–7.4), IBR loading amount (1.0–4.0 mg), and temperature (4.0–40.0 °C). A Franz diffusion cell was used for this aim whereas cellulose membrane having a cut-off as 12–14 kDa was used as the separator. After treating the membranes with a buffer solution (10 mM, pH 7.4) at room temperature overnight, they were placed between the parts of Franz cells while contacting a solution containing drug-loaded nanobubbles (1.0 mL) in the upper part and with the fresh releasing buffer solution (2.0 mL) in the lower part, where magnetic stirring was applied at 90 rpm to achieve homogeneity. Samples were taken from the bottom part of the Franz cell at the specified time intervals and the same volume of a fresh buffer solution was immediately added as the sample volume that was taken out. Separately, the solution containing the nanobubbles was immersed in a water bath in the release studies of nanobubbles after ultrasound treatment. The probe of the ultrasound device (Chattanooga, Intelect Mobile Combo – Model 2778, Texas, USA) has optional specifications in terms of frequency (1 MHz or 3 MHz), duty cycles (10%, 20%, 50%, continuous), pulse repetition rate (16, 48, or 100 Hz), and pulse duration (1–31.25 ms; max (ON): 31.25 ms, and min (OFF): 5 ms), which was also immersed in this water bath and activated at a 3 MHz frequency at 2 W cm^{-2} power density for 7 minutes. After this treatment step, the exploded nanobubbles were immediately be conducted to the release study as mentioned above. In order to quantify the IBR amount in the fresh solution, the samples collected at the specified time interval were measured with a UV-Vis spectrophotometer at a wavelength of 260 nm.

2.6. Mathematical modeling of release kinetics

The data obtained from the release studies with/without ultrasound treatment were analyzed by using well-established kinetic equations. Herein, three different models such as zeroth-order, first-order, and Korsmeyer–Peppas kinetic models were used to this aim as given below.

$$\text{Zero-order model: } q_t = q_0 + k_0 t \quad (1)$$

$$\text{First-order model: } \ln q_t = \ln q_0 - k_1 t \quad (2)$$

$$\text{Korsmeyer–Peppas model: } M_t/M_\infty = kt^n \quad (3)$$

where q_t is the amount of drug dissolved in time t, q_0 is the initial amount of drug in the solution and k_0 is the zero-order release constant expressed in units of concentration/time. In addition, M_∞ = cumulative drug amount released at the time, M_t = cumulative drug amount released at the time, M_t/M_∞ is a fraction of drug released at time t, k is the release rate constant and n is the release exponent, respectively.

2.7. Cytotoxicity studies

To demonstrate the cytotoxicity, in other words, biocompatibility, of the nanobubbles synthesized, a well-known 3-[4,5-dimethylthiazole-2-yl]-2,5-diphenyltetrazolium bromide test (MTT) assay was performed based on our previous studies.[26] We used the mouse fibroblast (L929) cell line as healthy cells and the human cervical (HeLa) cell line as soft cancer tissue cells. Herein, drug-free (bare) nanobubbles, drug-loaded nanobubbles, ultrasound-exploded drug-loaded nanobubbles, and free drug samples have interacted with the L929 cells and HeLa cells at different concentrations (5, 10, 25, 50, and 75 μM) for 24-hour incubation. Firstly, the samples were dissolved in ethanol and sterilized by UV radiation for 30 minutes. Samples in the different concentrations (5, 10, 25, 50, and 75 μM) were prepared in a cell culture medium. For the MTT assay, briefly, L929 cells (2×10^4 cells per mL) and HeLa cells (1×10^4 cells per mL) were planted in plates with 96 wells and incubated at 37 °C and 5% CO_2. After 24-hour incubation, the cells were treated with the samples given at the different concentrations mentioned above. After 24-hour treatment, an MTT assay was performed while measuring the absorbance (OD) values at 570 nm using a UV-visible spectrophotometer (EZ Read 400 Microplate Reader, Biochrom, UK). All values were reported as the mean ± standard deviation of six biological replicates. The percentage of cell viability is calculated using the following equation in accordance with the literature.[27] The morphological changes in the cells were analyzed utilizing an inverted microscope (IX70 Olympus, Japan).

$$\text{Cell viability (\%)} = [(\text{OD}_{\text{sample}} - \text{OD}_{\text{blank}})/(\text{OD}_{\text{control}} - \text{OD}_{\text{blank}})] \quad (4)$$

3. Results and discussion

3.1. Characterization studies

After the synthesis and washing-out processes of nanobubbles were completed, morphological and physico-chemical characterization studies were performed. First, the SEM observations were performed through two different approaches with/without a filtering step in order to assess their size, and size distribution from micro- and nano-scale (Fig. 2). Fig. 2A showed the nanobubbles before filtering whereas Fig. 2B showed them after filtration. In addition, drug-loaded nanobubbles were also investigated through SEM observations in order to evaluate the effects of drug loading on the size and size distribution of nanobubbles (Fig. 2C). The average sizes of the nanobubbles were calculated from SEM images by using a software, called ImageJ while counting and measuring the sizes of 25 nanobubbles and calculating their average size with standard deviation (SD). This calculation was applied for all samples such as drug-free (before and after the filtering process) and drug-loaded nanobubbles, separately. The average sizes of the nanobubbles were calculated as 353.2 ± 138.8 nm, 33.4 ± 11.4 nm, and 179.0 ± 29.1 nm, respectively. As observed in these images, the filtering process significantly decreased the size from 353.2 nm to 33.4 nm and resulted in a narrower size distribution, in which SD values decreased from ± 138.8 nm to ± 11.4 nm. These results figured out that the filtering step is necessary for getting rid of the larger (in micro-scale) nanobubbles to achieve the nanobubbles in the nanoscale with a narrower size distribution. In light of this observation, the nanobubbles were

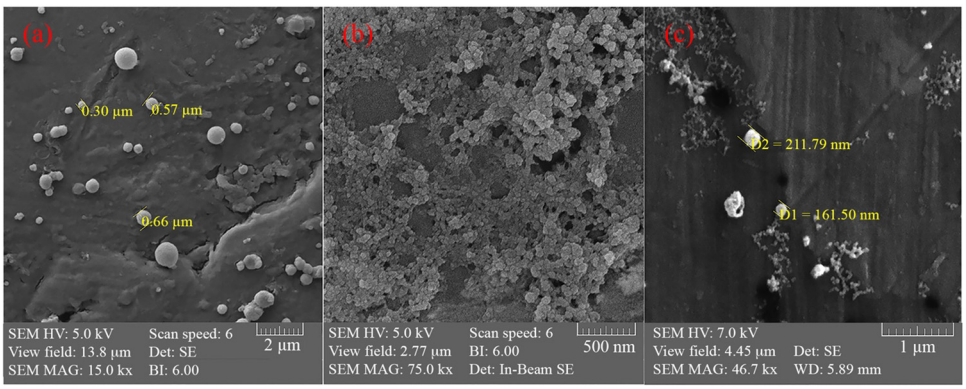

Fig. 2 SEM images of nanobubbles: (a) before filtering, (b) after filtering, and (c) drug loaded.

used after the filtering process for further steps. On the other hand, the drug-loading process caused an increase in terms of size. The size after the drug loading process was calculated as 179.0 nm with a relatively low size distribution of ±29.1 nm. This situation basically depended on the entrapment of drug molecules inside the nanobubbles and/or in between the polymeric shell and surfactant layer. Because the amount of ingredients inside nanobubbles increased, the force inside the nanobubbles increased as well, which resulted in enlarging the nanobubbles in terms of size.

The variation of size and size distribution of nanobubbles depended on the filtering and the drug loading process that was optimized by using four different feeding drug amounts as mentioned before. Furthermore, the zeta potential measurements of all nanobubbles were performed to evaluate the charge variation (ESI,† Fig. S1). The results are summarized in Table 1. It was observed that the zeta potential decreased negatively as the amount of the drug loaded into the nanobubbles increased. This increase is because as the drug enters the nanobubble, the proton donor/acceptor groups in the drug's structure direct the positive charge-providing functional groups of the collagen in the outer shell towards the inside. As a result of this orientation, the amount of positive charge sources on the outer surface decreases, resulting in the zeta potential value shifting to the negative region. The hydrodynamical diameters of the nanobubbles increased as the amount of drug loaded into the nanobubbles increased. Herein, it should be noted that the size of nanobubbles measured *via* SEM observation and zeta-size measurements was quite consistent. It is clearly seen that there is a non-significant difference only because of the principle of measuring the hydrodynamic diameter during the zeta-size analysis method. Furthermore, the stability and the presence of perfluoropentane in the gaseous core were evaluated with GC-MS studies (ESI,† Fig. S2–S5 and Table S1). The results revealed that nanobubbles have a gaseous core and a polymeric shell that exploded after ultrasound treatment. In addition, the power density (1 MHz or 3 MHz) of ultrasound treatment has no significant effect after 300 s treatment period (ESI,† Fig. S6).

Employing FTIR-ATR analyses, the functional groups of IBR, drug-loaded, and drug-free nanobubbles were investigated (Fig. 3). The characteristic bands of IBR were observed as the –N–H and the C–H stretching bands at 3344 cm^{-1} and 2972 cm^{-1}, respectively. Furthermore, the bands at 1565 cm^{-1}, 1474 cm^{-1}, and 1233 cm^{-1} correspond to the C=C–C, C=N, and CN stretching vibrations of the aromatic ring in the structure of IBR (Fig. 3a). When the FTIR-ATR results of drug-loaded nanobubbles were examined, it was observed that the characteristic bands of ibrutinib were observed herein as well (Fig. 3b). On the other hand, the drug-free nanobubbles do not have those characteristic bands related to the chemical structure of IBR except only aliphatic C–H stretching bands around 2970 cm^{-1} of the collagen, amide I/II stretching bands around 1650 cm^{-1} and ether/ester C–O–C bands around 1500 cm^{-1} were observed corresponding to polypeptide structure of collagen (Fig. 3c).[28] In conclusion, FTIR-ATR results revealed the chemical composition and successful loading of the drug molecules into the nanobubbles.

3.2. Drug loading capacity/efficiency

In order to calculate the drug loading efficiency, the calibration curve was plotted using the absorbance values of IBR concentration in the range of 0.1–10 mg mL^{-1} at 260 nm wavelength by spectrophotometry (ESI,† Fig. S7). The equation of the curve was calculated as $y = 0.0458x + 0.0073$ with a regression coefficient (R^2) of 0.9989. The loading efficiency of IBR-loaded nanobubbles was calculated by determining the amount of drug before (feeding solution) and after (washing-out solution) synthesis steps. The drug loading efficiencies of nanobubbles concerning the initial drug feeding amounts were 43.0%, 62.0%, 71.0%, and 87.0% for initial drug amounts in the range of 1.0–4.0 mg, respectively. Significantly increased drug loading and entrapment efficiency was obtained by the increasing the initial IBR concentration. Herein, the higher drug concentration forces the drug molecules to collect into the bubbles in the emulsion medium due to the concentration gradients between polar (aqueous) and non-polar (organic) phases and higher solubility in the organic phase (surfactants and solvent). The increase of loading more drug molecules into the bubbles lead to an increase in the diameter of the bubbles, which was also confirmed by SEM and zeta size analysis. In conclusion, it was observed that the amount of drug loaded into the

Table 1 Zeta-potential and zeta-size results of nanobubbles

IBR amount (mg)	Molecular structure of IBR	ZP (mV)	Average size, d (nm)	Polydispersity index
—	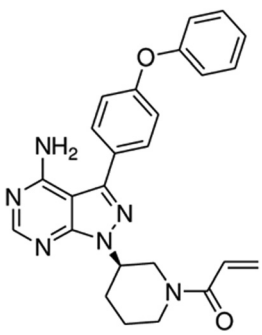	20.0	124.5 ± 9.5	0.359
1.00		18.4	136.2 ± 7.6	0.353
2.00		1.8	132.2 ± 6.0	0.358
3.00		−21.1	148.6 ± 5.1	0.313
4.00		−24.0	208.8 ± 5.1	0.468

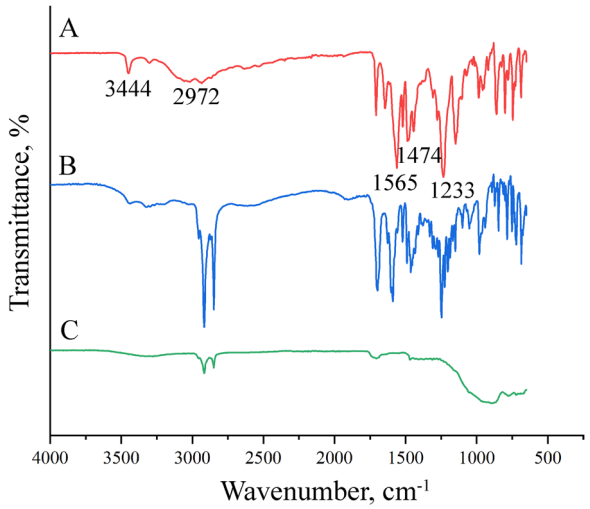

Fig. 3 FTIR-ATR spectra of (a) IBR, (b) drug-loaded, and (c) drug-free nanobubbles.

nanobubbles could be adjusted by varying the initial feeding amount concerning the final desired drug amount for carrying/releasing purposes.

3.3. Drug release studies

3.3.1. Without ultrasound treatment. Considering factors such as oxygen deficiency in cancer cells, the pH of the medium around the cancer tissue micro-environment differs from that of healthy cells.[29] Because of this difference between healthy and cancer tissue micro-environments, the researchers have developed pH-responsive drug delivery systems in related to pH-dependent drug release kinetics as well as pH-dependent carrier degradation.[30] Therefore, because of the unique and ubiquitous properties of tumor acidity among drug delivery systems, the use of pH-responsive nanocarriers in cancer therapy is prominent.[30] Furthermore, drugs are primarily released from pH-sensitive nanostructures due to processes such as swelling, cleavage, and protonation.[30]

In this respect, polypeptide-based polymeric (collagen) shell structures were preferred due to their strong pH-dependency besides their RGD repeating units for targeting the cancer tissue. During the profiling of the release rate, drug release studies were performed without ultrasound treatment to explode the bubbles. To this aim, release studies were performed with IBR-loaded nanobubbles at different pH (pH: 5.5; 6.0; 6.8; 7.0; 7.4) values for 6 days to determine the effect of pH on drug release performance (Fig. 4A). In the release study, it was observed that the drug release from the nanobubbles increased sharply in the first 2 hours (Fig. 4B), and subsequently established a linear kinetic until the 6th day. As a result of the release study, it was observed that the highest release occurred at pH 7.4. Herein, it was calculated that the bubbles released 31% of the drug in the first two hours at this pH whereas total up to 69% of the drug was released at the end of the 6th day after slowing down the releasing rate. The rapid drug release in the first stage is associated with the high drug concentration inside the nanobubble, which creates the concentration gradient between the inside and the outside of the bubble. Afterward, this concentration difference decreased relatively, and a drug release rate for the next six days (Fig. 4C) was almost equivalent to the amount of drug released only in the first two hours (Fig. 4D).

In addition, the effects of drug loading amount on the release kinetic were evaluated in this step. As seen in the Fig. 4C and D,

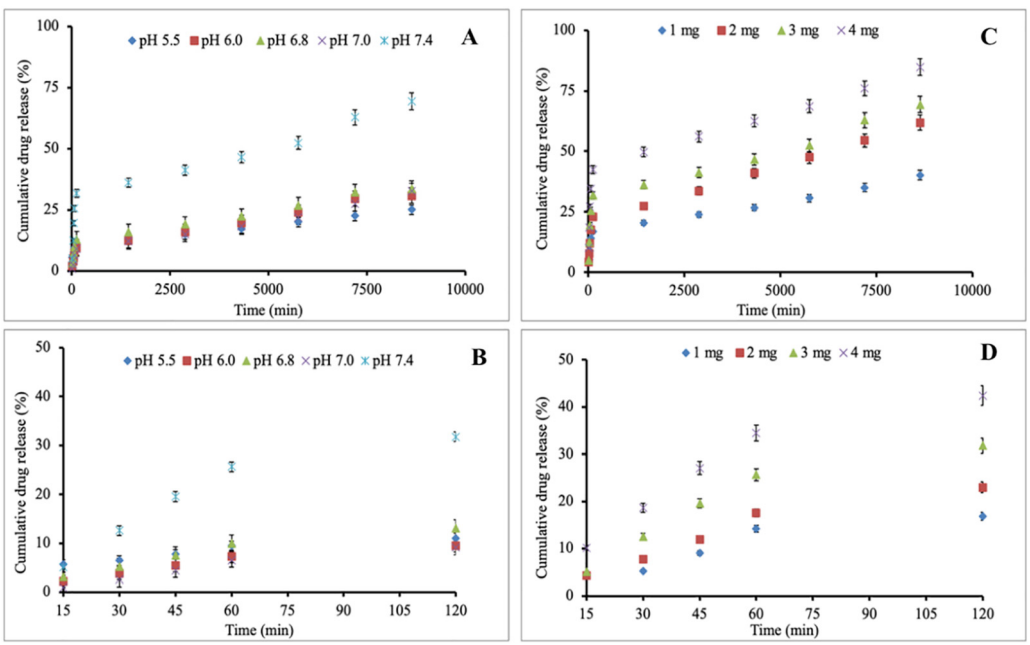

Fig. 4 Drug release profile of drug-loaded nanobubbles (A) at different pH values for 6 days and (B) for 120 min; at different drug concentrations (C) for 6 days and (D) for 120 min.

the increase in drug amount in the nanobubble also increased the cumulative amount of drug released as expected. In the first 2 h, the cumulative drug release rates of 1.0 mg, 2.0 mg, 3.0 mg, and 4.0 mg-loaded nanobubbles were calculated as 16.9%, 23.0%, 31.8%, and 42.4%, respectively. At the end of 6 days, these values were calculated as 40.1%, 61.9%, 69.4%, and 84.7% in the same order. According to the results, the increasing drug concentration had a significant effect on the cumulative amount of released drug, especially in the initial part of the drug release, which was directly related to the concentration gradient that caused internal pressure on the nanobubble's shell between the inside of the nanobubble and the environment. On the other hand, the effect of concentration on the amount of drug released during the longer release period (6 days) was determined to decrease relatively due to the diffusion-controlled release kinetics of the release model. This depended on the decrease in this concentration gradient and the establishment of the equilibrium situation.

Furthermore, a set of release studies was conducted at four different temperatures in order to determine the effect of temperature on drug release from nanobubbles. As given temperature-dependent drug release profiles (Fig. 5A and B) in the first 2 h, the cumulative release amount significantly increased by increasing temperature until 37.0 °C, then decreased at 40.0 °C. This result mainly depended on the interactions between drug molecules and polymeric shell, the boiling temperature of perfluoropentane (28.0 °C) used as a gas filler inside of the nanobubbles, the structural fluctuation of nanobubbles, and the conformational changes in the polypeptide-based structure of the collagen. The basic interactions were assumed as hydrogen bonds between the collagen groups forming the outer shell of the nanoballs and drug molecules, which were weakening by increasing temperature; in other words, the drug molecules escaped more easily. However, other factors may compete with these main forces and change the drug release profile at higher temperatures. As mentioned before, there was an unexpected significant increase in the cumulative release amount after the 3rd day (4320 min) at 40.0 °C. To reveal the reason for this behavior, a set of experiments to evaluate the structural stability of the nanobubbles was performed. These results may be related to the temperature of the release environment having undesired effects on the structural uniformity of the nanobubbles which might deteriorate under this situation. Accordingly, the sizes of the nanobubbles were separately analyzed at 37.0 °C and 40.0 °C on days 2–4 to observe the structural change and the structural degradation.

To confirm the temperature-structural stability, the size analyses of nanobubbles in release environments at 37.0 °C and 40.0 °C were performed just before degradation (2 days, 2880 min), at the beginning of degradation (3 days, 4320 min), and after degradation (4 days, 5760 min) (Fig. 5C and D). According to the size analyses, there was no degradation in the nanobubbles released in the release environment at 37.0 °C whereas a deterioration effect of the temperature on the nanobubbles was observed at 40.0 °C. As no significant variation was observed during evaluation at 37.0 °C (Fig. 5C) there was no change in the size and size distribution of the nanobubbles. In contrast, it was observed that there is an adverse effect of temperature (40.0 °C) on the nanobubble size, size distribution, and structural stability as enwidening in the size and formation of new size peaks in the zeta-size curve (Fig. 5D).

3.3.2. With ultrasound treatment. Ultrasound increases the permeability of biological barriers such as cell membranes and blood–brain barriers by triggering vibrations in the fluid medium, increasing the kinetic energy and thus increasing the

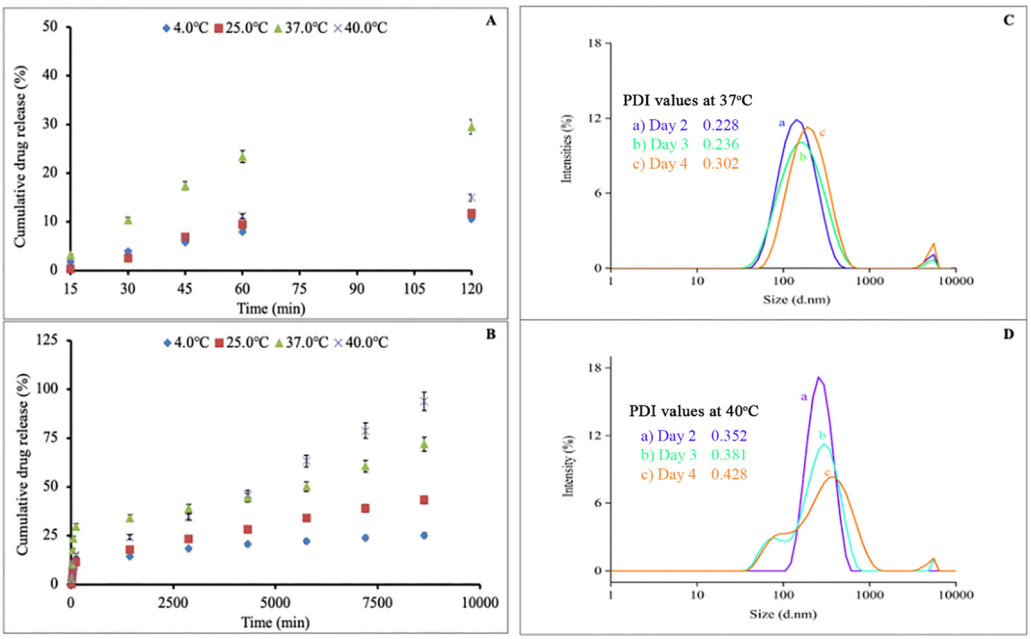

Fig. 5 Temperature-dependent drug release profile for (A) first 120 min and (B) 6 days. Size analysis of nanobubbles to assess thermal stability at (C) 37.0 °C and (D) 40.0 °C for (a) 2 days, 2880 min, (b) 3 days, 4320 min, and (c) 4 days, 5760 min.

ambient temperature.[31,32] In light of this well-known phenomenon, drug release studies were performed after treating the nanobubbles with ultrasound. Herein, three effecting parameters including pH, drug-loading amount, and temperature were evaluated in parallel with the previous experimental set. The release of ultrasound-exploded nanobubbles in the first 24 hours is considerably higher than that of ultrasound-untreated nanobubbles as expected.

When the pH study was examined, it was observed that the pH-dependency of the drug release kinetic in the case of ultrasound-exploded nanobubbles was similar to that of ultrasound-untreated nanobubbles while the highest cumulative release amount was achieved at pH 7.4 (Fig. 6A). In the pH range (pH: 5.5, 6.0, 6.8, 7.0, and 7.4), the cumulative drug release amounts during 24 h-releasing period were, respectively, determined as 13.0%, 12.5%, 16.1%, 12.3%, and 36.1% for ultrasound-untreated nanobubbles whereas they were determined as 36.9%, 46.3%, 52.7%, 37.4%, and 66.9% in the same order for ultrasound-exploded nanobubbles. The results showed that ultrasound has a significant effect on drug release from nanobubbles while allowing an almost 2.5–3.0-fold increase in the released drug amount. It clearly figured out that ultrasound treatment exploded the nanobubbles and deteriorated their structural uniformity which allowed drug molecules to burst-release into the environment.

As a second effecting parameter, the amount of drug loaded into nanobubbles was investigated for the 24-hour releasing process. Herein, nanobubble samples having four different drug amounts were exploded *via* ultrasound treatment before the release experiment as mentioned before (Fig. 6B). In parallel with previous results, the increase in the loaded amount of the drug caused an increase in the release percentage. Cumulative drug release rates were calculated as 39.4%, 52.2%, 66.8%, and 75.3% for the feeding drug amount varied as 1.0, 2.0, 3.0, and 4 mg at 24 h, respectively. The increase in the rate is closely related to the amount of the drug inside nanobubbles because the explosion by ultrasound treatment allowed drug molecules to be free from the nanobubbles more easily and rapidly be released into the environment, which resulted in a higher concentration, in other words, higher cumulative release rate.

As a third effecting parameter, the temperature was varied in the range of 4.0–40.0 °C, the same as in the previous experiment for 24 hours (Fig. 6C). The drug release results as shown in Fig. 6C revealed that the most appropriate temperature was 37.0 °C according to the highest cumulative release rate. Herein, two interesting outcomes should be mentioned: the first, the cumulative release rate observed at 40.0 °C was lower than that at 37.0 °C. This result pointed out that not only the structural uniformity of the nanobubbles but also the interactions (between the drug and the polymeric shell) and conformation of the polymeric shell influenced the release rates. Moreover, the explosion disrupted the nanobubbles in combination with the temperature effect as discussed before; however, the polymeric residues may create smaller shells around drug molecules or strongly bind the drug molecules, which direct drug diffusion was limited under both situations. Secondly, the drug molecules might be loaded both in the inside of nanobubbles and in between shell and surfactant molecules. In conclusion, the temperature of the releasing environment is one of the key factors in adjusting the cumulative drug release amount with respect to the desired amount of the drug to be released.

3.4. Mathematical modeling of release kinetics

The data obtained from the drug release studies were modeled by using three well-established mathematical equations as

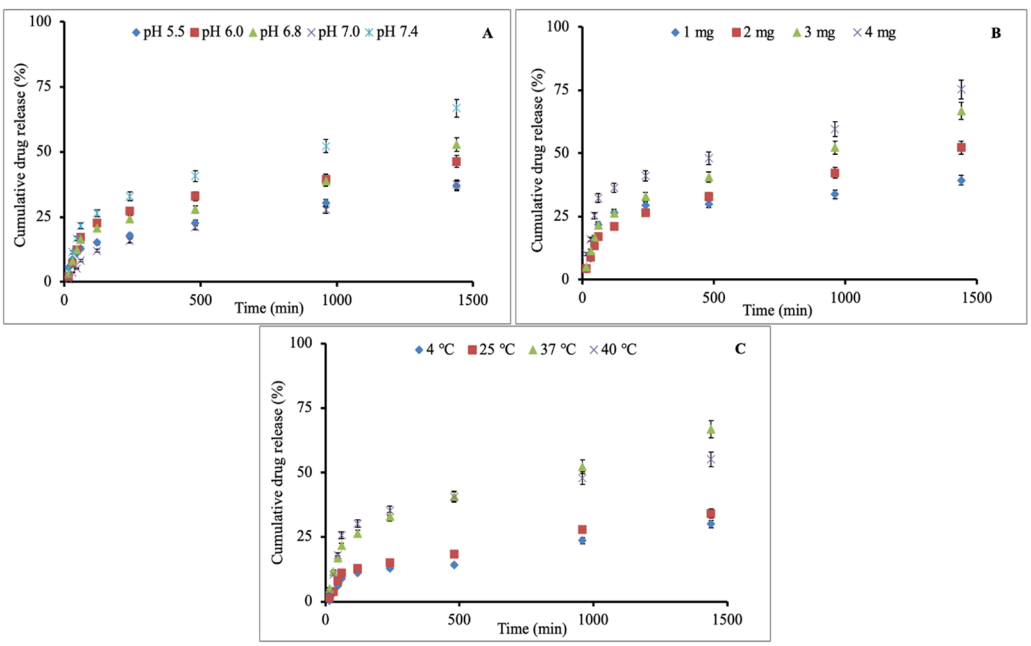

Fig. 6 Drug release profiles after ultrasound explosion. The evaluation of (A) pH-dependency (IBR amount: 3.0 mg and *t*: 37.0 °C), (B) concentration-dependency (pH: 7.4 and t: 37.0 °C), and (C) temperature-dependency (pH: 7.4 and IBR amount: 3.0 mg).

Table 2 Mathematical modeling of drug release kinetics results

Parameters		pH	n	Regression coefficient, R^2		
				Korsmeyer–Peppas	Zeroth-order	First-order
Without ultrasound	For the first 120 min	5.5	0.42	**0.96**	0.83	0.74
		6.0	0.73	**0.97**	0.91	0.78
		6.8	0.70	**0.98**	0.92	0.80
		7.0	1.08	**0.96**	0.93	0.75
		7.4	0.90	**0.93**	0.85	0.68
	From day 1 to day 6	5.5	0.33	0.96	**0.99**	**0.99**
		6.0	0.53	0.97	**0.99**	0.97
		6.8	0.43	0.95	**0.98**	**0.98**
		7.0	0.54	0.94	0.98	**0.99**
		7.4	0.36	0.92	0.98	**0.99**
With ultrasound		5.5	0.37	**0.98**	0.93	0.74
		6.0	0.55	**0.83**	0.79	0.45
		6.8	0.51	0.89	**0.91**	0.58
		7.0	0.68	0.89	**0.92**	0.56
		7.4	1.04	**0.99**	0.90	0.93

mentioned before (Table 2) while the respective figures are given in ESI† (Fig. S8–S11). Herein, the data were categorized into two main rows: with/without ultrasound treatment. The drug releasing data without ultrasound treatment were analyzed in details with respect to both the first 2 h (0–120 min) and 6 days (1440–8640 min) because the first releasing period was observed as burst and steeply kinetic while differing from the general releasing profile. In the case of ultrasound-untreated nanobubbles, the release kinetic mainly depended on the diffusion of drug molecules from the polymeric shell where they were entrapped or inside of the nanobubbles where they were encapsulated. In the first section of the table (for the period of 0–2 h), the release kinetics parameters at different pH environments were analyzed employing the zeroth-order, first-order, and Korsmeyer–Peppas kinetic models. It was observed that ultrasound-untreated nanobubbles showed different pH-dependent releasing kinetics. They followed the Fickian diffusion law at pH 5.5 whereas they showed non-Fickian release behavior at pH values of 6.0 and 6.8 with the introduction of the swelling effect. Differently, super case II range behavior was observed at pH values of 7.0 and 7.4 with respect to the calculated n values ($n > 0.89$). These results pointed out that there is no single parameter like pH-dependent interaction through complementary charges to control the release profile. However, a combination of parameters including intermolecular interaction, swelling, structural stability, and conformation cooperated to determine the release kinetic profile as discussed before. In the second section (from day 1 to day 6), diffusion-controlled release kinetics were dominant at pH values of 5.5 and 7.4 (Fickian behavior) whereas simultaneous diffusion- and swelling-controlled release kinetics were determined at pH values of 6.0, 6.8, and 7.0 (non-Fickian behavior). With respect to the regression coefficients (R^2), both release kinetics are consistent with the Korsmeyer–Peppas kinetic model for the first 2 h whereas zeroth-order kinetic at lower pH values and first-order kinetic at higher pH values were observed for 6-days releasing data. In the third section of the table, the data for ultrasound-treated nanobubbles were analyzed within the first 24 h-releasing period. Similar to untreated nanobubbles, treated nanobubbles followed diffusion-controlled release kinetic (Fickian behavior) at only pH 5.5. However, diffusion- and swelling-controlled (non-Fickian behavior) was observed at wider pH ranges as 6.0, 6.8, and 7.0. Interestingly, super case II behavior was dominant at pH 7.4 because only swelling gained importance after the explosion process exposed the glassy polymeric fragments. In general, diffusion control the releasing process at lower pH values due to the interaction balance between protonated–deprotonated groups on the poly-peptide based polymer and the drug. Therefore, diffusion (especially at pH 5.5) still acted as a limiting factor, although the integrity of the polymeric shell disappeared after the explosion. At intermediate pH values (pH 6.0 to 7.0) the effect of diffusion as well as polymer swelling and drug dissolution became more pronounced. In the last part (pH 7.4), the interaction strength of the interacting groups decreases, and an effective release (super case II) profile is established.

3.5. Cytotoxicity studies

For the MTT assay, L929 cells and HeLa cells were treated with drug-free (bare) nanobubbles, drug-loaded nanobubbles, ultrasound-exploded drug-loaded nanobubbles, and free drug at different (5, 10, 25, 50, and 75 μM) concentrations. MTT results showed that drug-free nanobubbles did not adversely affect cell viability and drug-loaded materials caused a decrease in viability at increasing concentrations for both healthy and cancer cell lines (Fig. 7 and 8). L929 cell viability was close to that of the control group in the drug-free nanobubble group. However, there was a decrease in cell viability with increasing concentration in the drug-loaded nanobubbles, ultrasound-exploded drug-loaded nanobubbles, and free drug groups especially above 25 μM (Fig. 7).

HeLa cell viability remained close to 100% in the control group and the drug-free nanobubble group, which revealed that the drug-free nanobubbles were also harmless in HeLa cells identical to L929 cells (Fig. 8). This result indicated that anti-cancer or toxicity effect of nanobubbles were not stemmed from polymeric shell collagen. On the other hand, a significant dose-dependent decrease in cell viability was observed in the

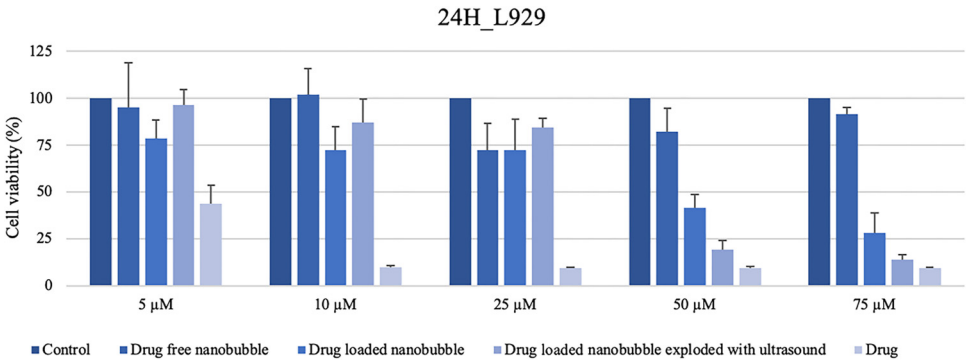

Fig. 7 L929 cell viability results of drug-free, drug-loaded, ultrasound-exploded nanobubbles, and free drug solutions at different concentrations for 24 hours. Drug-loaded nanobubbles with/without ultrasound treatment showed a cytotoxic effect with increased concentration that is parallel to IBR treatment. All values were expressed as the mean ± standard deviation of six biological replicates. The percentage of cell viability is calculated using following the equation stated in Section 2.7.

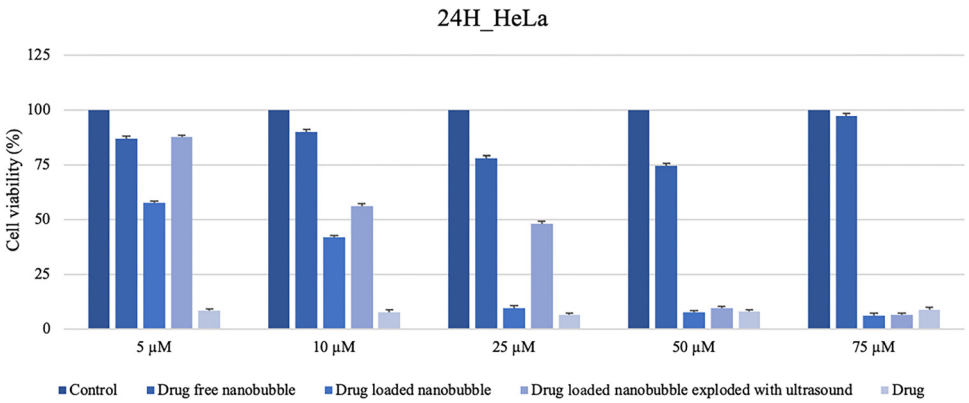

Fig. 8 HeLa cell viability after treatment with drug-free, drug-loaded, ultrasound-exploded nanobubbles, and free drug solutions at different concentrations for 24 hours. Drug-loaded nanobubbles with/without ultrasound treatment showed higher drug-release efficiency with increased concentration, causing a significantly decreased cell viability for HeLa cells. All values were expressed as the mean ± standard deviation of six biological replicates.

drug-loaded nanobubbles. Beginning at 5 μM, the drug groups started to show an anti-cancer effect, which became more significant as the drug concentration increased. Especially at a concentration of 75 μM, cell viability decreased below 25%, emphasizing the strong antiproliferative effect of IBR. Furthermore, ultrasound-exploded nanobubbles showed a similar anti-cancer effect on the free drug group and drug-loaded nanobubbles, as they allowed controlled drug release. A significant decrease in cell viability was observed even at low concentrations, indicating that ultrasound-assisted drug release is more effective than without ultrasound treatment. Especially at high concentrations, cell viability decreased below 25%. Overall, the viability results showed a dose-dependent increase in the anti-cancer effect. The cell death rate at high concentrations (50 μM and above) in the free drug and drug-loaded nanobubble groups is quite high, proving that IBR shows a strong antiproliferative effect on HeLa cells. These results indicated that IBR effectively induces cell death when applied with nanobubble-based delivery systems whereas ultrasound-exploded nanobubbles are effective in controlled drug release at higher concentration, especially.

As given in the ESI† file (Fig. S12 and S13), optical microscopy images observed in both cell culture studies verified that increased concentrations caused morphological changes for both cell lines, especially for HeLa cells. Both cell types typically exhibit an epithelial-like morphology. While this morphology was maintained in the control group, significant alterations were observed in the morphology of cells in the increased concentrations, particularly in the HeLa cells. L929 cell morphology was changed to a round form with higher concentrations of drug-loaded, ultrasound-exploded nanobubbles, and free drug while control cell morphology was preserved in the drug-free nanobubble group (Fig. S12, ESI†). HeLa cells also lost their natural morphology and adopted a round shape for higher concentrations of drug-loaded, ultrasound-exploded nanobubble group while in the free drug group the death cell number was increased and the cell morphology couldn't be observed. Control cell morphology was preserved in the drug-free nanobubble group for HeLa cells (Fig. S13, ESI†). The morphological changes of cells supported viability results. Furthermore, the drug-free nanobubbles didn't exhibit any cytotoxic effect on both cell lines showing almost the same cell

viability as the control group. In line with this result, it is possible to say that perfluoropentane used in the internal gas structure of the bubbles does not show any cytotoxic effect at low concentrations.[33] According to the MTT results of drug-loaded nanobubbles with/without ultrasound treatment, it was observed that the cytotoxic effect increased as the concentration increased in parallel with IBR treatment. The difference in cell viability between the drug-loaded nanobubbles with/without ultrasound and IBR has resulted from the controlled release of IBR from the nanobubble system. IBR, Bruton's tyrosine kinase inhibitor, shows antiproliferative effects on cells, especially human ovarian, breast, and lung cancers.[34] For this reason, at concentrations as low as 5 μM, IBR was found to have a cytotoxic effect on both cell lines, which increased with concentration. At higher concentrations (above 25 μM for L919 cells and above 5 μM for HeLa cells), ultrasound-treated nanobubbles showed similar activity to IBR. With increasing drug loading concentration and ultrasound treatment, the cytotoxic activities became similar. It can be concluded that the IBR-loaded nanobubble system has a parallel cytotoxicity pattern to free IBR. The findings from the HeLa cell culture study suggest that nanobubble systems have the potential to be highly efficacious in the context of passively targeted and controlled drug release for soft tissue cancer cells.

4. Conclusions

Targeting only the tumor side, decreasing side-effects of chemotherapeutics, and increasing their solubility and bioavailability are major and challenging issues not only for cancer therapy but also controlled drug releasing research. Because most of chemotherapeutics have hydrophobic nature and are easily metabolized, they must be administered in a higher amount more than enough for complete curing the illness. Therefore, increasing their solubility may extend their bioavailability; however, administering a higher amount damages tumor issue as well as healthy cells through the circulation. In this respect, a triplex approach attracts researchers' attention to overcome undesired effects of chemotherapeutics. Herein, a synergetical strategy was developed by utilizing/combining the passive-targeting feature of collagen, high efficiency of IBR, and good penetration and ultrasound-responsivity of nanobubbles. The developed collagen nanobubbles showed superior properties in terms of increasing solubility of IBR, controlled release of the cargo agent, and cell targeting. In the case of no ultrasound treatment, the release kinetic studies revealed out that a burst release behavior was observed for first 2 hours whereas a first-order release kinetics was determined for further time frame of up to 6 days, when almost 70% percent of loaded drug was released. On the other hand, the similar cumulative releasing performance was achieved in only 24-hours with ultrasound treatment. Furthermore, the developed nanobubbles have biocompatibility in the light of cell culture study results. In addition, a critical drug level was observed as 50 μM, in which drug-loaded nanobubbles behave as a free drug after ultrasound treatment. In addition, the cytotoxicity test served as a basic data source for further *in vivo* studies. In conclusion, it should be mentioned that the nanobubbles has a potential for targeted controlled delivery for IBR with the aim of safer, cheaper, and efficient chemotherapy, especially of soft tissue tumors like lymphoma or breast cancer.

Data availability

The data supporting this article have been included as part of the ESI.†

Conflicts of interest

There are no conflicts to declare.

References

1 C. Alvarez-Lorenzo and A. Concheiro, *Fundam. Smart Mater.*, 2020, 170.
2 M. N. Ravi Kumar and N. Kumar, *Drug Dev. Ind. Pharm.*, 2001, **27**, 1–30.
3 S. R. Motamedian, S. Hosseinpour, M. G. Ahsaie and A. Khojasteh, *World J. Stem Cells.*, 2015, **7**, 657–668.
4 K. J. Rambhia and P. X. Ma, *J. Controlled Release*, 2015, **219**, 119–128.
5 J. Cao, D. Huang and N. A. Peppas, *Adv. Drug Delivery Rev.*, 2020, **167**, 170–188.
6 I. Keklikoglou, C. Cianciaruso, E. Güç, M. L. Squadrito, L. M. Spring, S. Tazzyman, L. Lambein, A. Poissonnier, G. B. Ferraro and C. Baer, *Nat. Cell Biol.*, 2019, **21**, 190–202.
7 Q. Qiu, M. Lu, C. Li, X. Luo, X. Liu, L. Hu, M. Liu, H. Zheng, H. Zhang and M. Liu, *AAPS PharmSciTech*, 2018, **19**, 3571–3583.
8 C. Armutcu, *Turk. J. Chem.*, 2022, **46**, 1632–1641.
9 V. Zvonicek, E. Skorepova, M. Dusek, M. Babor, P. Zvatora and M. Šoš, *Cryst. Growth Des.*, 2017, **17**, 3116–3127.
10 J. H. Phan, R. A. Moffitt, T. H. Stokes, J. Liu, A. N. Young, S. Nie and M. D. Wang, *Trends Biotechnol.*, 2009, **27**, 350–358.
11 K. Wong and X. Liu, *Pediatr. Surg. Int.*, 2012, **28**, 943–951.
12 R. Cavalli, M. Soster and M. Argenziano, *Ther. Delivery*, 2016, **7**, 117–138.
13 D. V. Batchelor, F. J. Armistead, N. Ingram, S. A. Peyman, J. R. McLaughlan, P. L. Coletta and S. D. Evans, *Langmuir*, 2022, **38**, 13943–13954.
14 R. Pasupathy, P. Pandian and S. Selvamuthukumar, *Braz. J. Pharm. Sci.*, 2022, **58**, 1–22.
15 R. Xiong, R. X. Xu, C. Huang, S. De Smedt and K. Braeckmans, *Chem. Soc. Rev.*, 2021, **50**, 5746–5776.
16 T. Li, J. Zhou, C. Zhang, X. Zhi, J. Niu, H. Fu, J. Song and D. Cui, *NPG Asia Mater.*, 2018, **10**, 1046–1060.
17 P. Nittayacharn, H.-X. Yuan, C. Hernandez, P. Bielecki, H. Zhou and A. A. Exner, *J. Pharm. Sci.*, 2019, **108**, 3091–3098.
18 N. Maghsoudnia, R. B. Eftekhari, A. N. Sohi, A. Zamzami and F. A. Dorkoosh, *J. Nanopart. Res.*, 2020, **22**, 1–41.

19 S. B. Keller and M. A. Averkiou, *Bioconjug. Chem.*, 2021, **33**, 1049–1056.
20 B. An, Y.-S. Lin and B. Brodsky, *Adv. Drug Delivery Rev.*, 2016, **97**, 69–84.
21 B. Leitinger and E. Hohenester, *Matrix Biol.*, 2007, **26**, 146–155.
22 T. Karasu, F. Z. Erkoc-Biradli, M. Ö. Öztürk-Öncel, C. Armutcu, L. Uzun, B. Garipcan and M. E. Çorman, *Biomed. Phys. Eng. Express*, 2022, **8**, 055004.
23 M. Li, Y. Wang, M. Li, X. Wu, S. Setrerrahmane and H. Xu, *Acta Pharm. Sin. B*, 2021, **11**, 2726–2737.
24 M. Nieberler, U. Reuning, F. Reichart, J. Notni, H.-J. Wester, M. Schwaiger, M. Weinmüller, A. Räder, K. Steiger and H. Kessler, *Cancers*, 2017, **9**, 1–33.
25 E. Ruoslahti and M. D. Pierschbacher, *Science*, 1987, **238**, 491–497.
26 C. Akay, M. Ç. Taniş and H. Sevim, *Int. J. Artif. Organs.*, 2017, **40**, 581–588.
27 M. Çakırbay Tanış, C. Akay and H. Sevim, *Int. J. Artif. Organs*, 2018, **41**, 677–683.
28 X. Shi, C. Wang, Q. Chen, S. Shen, S. Song and X. Zhou, *J Drug Deliv Sci Technol.*, 2021, **63**, 102554.
29 B. A. Webb, M. Chimenti, M. P. Jacobson and D. L. Barber, *Nat. Rev. Cancer*, 2011, **11**, 671–677.
30 F. Danhier, O. Feron and V. Préat, *J. Controlled Release*, 2010, **148**, 135–146.
31 E. C. Unger, T. P. McCreery and R. H. Sweitzer, *Invest. Radiol.*, 1997, **32**, 723–727.
32 S. R. Sirsi and M. A. Borden, *Adv. Drug Delivery Rev.*, 2014, **72**, 3–14.
33 S. Zullino, M. Argenziano, I. Stura, C. Guiot and R. Cavalli, *Mol. Imaging*, 2018, **17**, 1536–1552.
34 J. Wang, X. Liu, Y. Hong, S. Wang, P. Chen, A. Gu, X. Guo and P. Zhao, *J. Exp. Clin. Cancer Res.*, 2017, **36**, 1–13.